Energy loss of fast clusters through matter

D. Ben-Hamu, A. Baer, H. Feldman, J. Levin, O. Heber, Z. Amitay, Z. Vager, and D. Zajfman
Department of Particle Physics, Weizmann Institute of Science, Rehovot 76100, Israel
(Received 5 June 1997)

Energy loss in the MeV range of simple clusters impinging on thin carbon targets has been measured using a time-of-flight method. Stopping-power ratios defined as the ratio of the stopping power of the cluster to the sum of the stopping powers of the constituent atoms moving at the same velocity were investigated. Stopping-power ratios close to unity were observed for O_2 and B_3 clusters, while deenhancement effect is observed in the stopping-power ratios of C_3 and C_4. The experimental results are compared both with an existing theoretical model, which takes into account the spatial correlation of the fragments, and with a simple united-atom model, which also includes the charge state evolution of the fragment ions inside the target. [S1050-2947(97)10711-9]

PACS number(s): 34.50.Bw

I. INTRODUCTION

The penetration of fast clusters through matter has been a subject of great interest during recent years. Heavy ion clusters have been suggested to provide the initial step for the production of energy from nuclear fusion reactions by the inertial confinement fusion (ICF) process [1]. This idea is based on the seemingly large energy deposition by the cluster in the solid material as compared to the individual atoms moving at the same velocity. Molecular effects on the electronic energy loss have been theoretically studied for fast clusters moving in various media. Basbas and Ritchie [2] have studied the energy loss of diclusters in a valence electron gas in the dielectric approach using a simple dielectric function to describe single particle and collective excitations of the electrons in the gas. Enhancement effects in the energy loss of the cluster were found for small values of the parameter $r\omega_p/v$, where r is the internuclear distance, v is the cluster velocity, and ω_p is the plasma frequency of the electrons in the gas. Similarities were found by these authors for the energy loss of clusters to classical harmonically bound electrons, where constructive interference effects were expected to occur for small values of $r\omega/v$, where in this case, the plasma frequency ω_p has been replaced with the transition frequency ω of the harmonic oscillator. Basbas and Ritchie have also studied the energy loss of clusters due to collisions with single atoms using a quantum-mechanical perturbation theory. Vicinity effects were found to excitations from $1s$ hydrogenic orbitals and excitations from $2s$ and $2p$ aluminum orbitals. The energy loss of clusters in a free electron gas has been studied by Arista [3] using Lindhard's dielectric function [4]. Enhancement effects are expected to occur for small internuclear distances, as a result of interference effects in the response of target electrons to the fields of the moving ions in the cluster.

On the experimental side, cluster effects have been observed in point defect creation in LiF crystal bombarded with C_3 and C_5 clusters at energies of 1.74 MeV/atom when compared to those produced by irradiation with single C ions with the same respective energy and dose. The enhanced defect production was explained to be the result of the high density of electronic excitations near the surface of the sample when the tracks associated with each carbon atom of the cluster overlap [5]. Molecular effects have also been observed in secondary ion emissions from surfaces of organic and inorganic thin films bombarded by clusters. Enhanced secondary ion yields induced by MeV ionic gold cluster bombardment were observed relative to single gold ions moving at the same velocity [6].

The most intensive experimental and theoretical works have been carried out in the field of energy loss of molecular projectiles passing through solid targets. Enhancement effects in the stopping powers have been observed for fast hydrogen clusters moving at velocities above the Bohr velocity. The magnitude of the effect, however, differs significantly for different experiments and varies from less than 10% to more than 50% [7–11]. Energy losses have also been measured for diatomic N_2^+ in the energy range of 0.5 to 1.8 MeV/atom and for O_2^+ at energies of 1.0 and 1.6 MeV/atom. The molecules were selected so that their axis was aligned with the beam direction, showing in this case a deenhancement effect on the stopping power relative to single ions having the same velocity as the cluster [12]. The stopping-power ratio of 1.6 MeV/atom O_2^+ measured by these authors was found to be $R=0.95$, showing slight deenhancement while a value as high as $R=1.45$ was reported by others [13]. Recent measurements of carbon clusters C_n $(n=2-8)$ in the energy range of 2.275–5.65 MeV/atom show a small enhancement effect in the stopping power of the cluster relative to single carbon ions at the same velocity [14].

In a few of the above experiments, energy-loss measurements were carried out using energy-sensitive detectors such as surface barrier detectors. It is well known that these devices suffer from deviations when energy is measured for cluster impact and compared to single particle impact. These deviations have been termed pulse height defect (PHD) and are the result of several processes. Among these, one can cite the nuclear stopping, which does not lead to electron-hole pairs, the energy loss at the surface of the detector due to the dead layer, and the incomplete charge collection in the detector due to plasma recombination [15]. Hence, corrections are generally needed in order to obtain the accurate energy of the molecular projectile. These corrections are sometimes of the same order of magnitude as the effect to be measured.

In the present work, we have measured the energy loss of several simple clusters using a time-of-flight technique. In

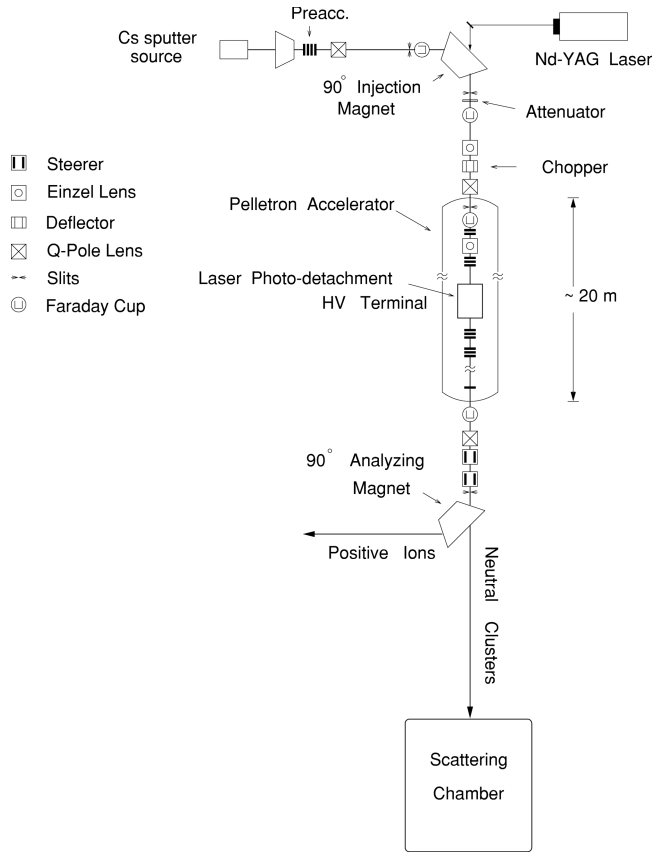

FIG. 1. Experimental setup for fast neutral molecular beam source.

this technique, the time of flight of the cluster projectile is measured along a field-free region after passing through the target. The technique has the advantage of measuring energy losses directly without any detector effects as in the case of surface barrier detectors, and thus no corrections are needed. Stopping powers of 11.3-MeV O_2 and 11.6-MeV B_3, C_3, and C_4 have been measured in carbon targets ranging in thicknesses from 4 to 50 μg/cm^2. The results are compared to a theoretical model developed by Arista, and to a united-atom model elaborated upon here. The united atom model is also compared to previous experimental results measured by other authors.

II. EXPERIMENTAL METHOD

A. Fast neutral beams

Fast neutral molecules are produced using the existing experimental setup for Coulomb explosion imaging (CEI) [16,17], shown in Fig. 1. A negative molecular ion beam is generated by a cesium sputter source, extracted first by a potential difference of 10 kV and further accelerated by an additional 90 kV potential difference. After being mass selected by the injection magnet (see Fig. 1) the ions are chopped to a time width of $\sim$400 ns and then injected into the 14UD Pelletron accelerator where the beam energy is boosted to a value of 11.6 MeV. The time width of the ion pulses as produced by the chopper is selected so that the corresponding length of the accelerated ion pulse is smaller than the length of the field-free region of the high voltage

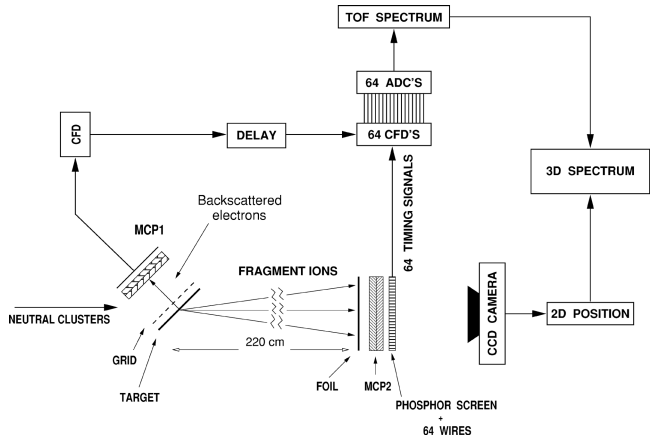

FIG. 2. Experimental setup for time-of-flight measurements. The drawing is not to scale.

(HV) terminal (3 m). When the ions reach the HV terminal at the center of the accelerator, a laser pulse (Nd-YAG, $\lambda = 532$ nm) is fired in order to neutralize the negative molecular ions by a photodetachment process. The resultant high-energy neutral molecules drift along the second section of the accelerator unaffected by the potential difference. Any charged ions that are left in the beam are purged by the 90° analyzing magnet (see Fig. 1). The neutral molecules that pass unaffected by the 90° analyzing magnet are directed toward the time-of-flight and scattering chamber where the targets are located.

B. Time-of-flight measurement

The experimental setup for a time-of-flight measurement is depicted in Fig. 2. Fast neutral clusters reaching from the accelerator are incident upon a thin carbon foil with its normal oriented 45° relative to the beam direction. Within a few angstroms of penetration into the target, the cluster loses most of its binding electrons due to the large cross section for electron stripping. The resultant charged nuclei rapidly separate due to their mutual Coulomb repulsion, converting their initial electrostatic energy into kinetic energy of their relative motion. Their motion inside the target is influenced by collisions with target atoms. In these collisions, the fragment ions are scattered from the target nuclei. Subsequently, their charge states may change by electron loss and electron capture processes, and they may lose energy to the target atoms by elastic and inelastic collisions. After passing through the target, the fragment ions emerge into the vacuum, along the 220-cm field-free region and hit a three-dimensional (3D) position- and time-sensitive detector. The time of impact as well as the position on the surface of the detector are measured for all the fragments of a simple molecule, one molecule at a time. The time at which the cluster impacts upon the target is used as a reference time. This signal is generated by the backscattered electrons from the target surface induced by the cluster impact. These electrons are accelerated toward a microchannel plate (MCP1 in Fig. 2) by applying an accelerating voltage of 2 kV between a 81% transmission grid and the target.

The 3D detector [16] consists of a charge-coupled device (CCD) camera located outside the vacuum chamber, together with a microchannel plate detection system made of three

layers. The first layer consists of an aluminized Mylar foil coated with CsI, and is used to increase the detection efficiency by generating a few tens of electrons for each fragment impact. These electrons are then accelerated by a potential difference of 200 V toward an 80-mm-diam chevron assembly microchannel plate (MCP2) located 2 mm below the aluminized Mylar foil. The third layer, located 3 mm away from the microchannel plate, consists of 64 wires that are located 0.2 mm above a glass window coated with a phosphor layer. The electrons created at the back side of the microchannel plate are accelerated by a potential difference of 2 kV toward the wires and the phosphor screen. The induced signals on the wires are used as timing signals for each fragment hit. Each of these timing signals is fed, after shaping and amplification, into a constant fraction discriminator (CFD). The CFD serves as a constant current source for a charge analog-to-digital converter (ADC). These current sources are switched off by the delayed signal coming from MCP1 (see above). Each electron bunch hitting the phosphor screen generates a spot of ~ 1 mm diameter. These are recorded by a CCD camera viewing the screen through a sealed window. Thus for each cluster, the time of arrival of each of the fragment ions is measured relative to the time of impact of the cluster on the target. The position of each of the fragments on the detector surface is also recorded. Since the time of flight of each of the molecular fragments is measured for each molecule, the time of flight of the center of mass of the molecule, which is essentially the quantity of interest in the present case, can be determined.

To show that, consider a cluster of N atoms moving along a field-free region of length L after passing through a thin target. The total energy of the cluster in the laboratory frame of reference is given by

$$E=\frac{1}{2}\sum_{i}^{N} m_i V_i^2=\frac{L^2}{2}\sum_{i}^{N} m_i\left(\frac{1}{t_i}\right)^2, \tag{1}$$

where V_i is the velocity of the ith atom in the laboratory frame of reference and t_i is its time of flight along the field-free region. For thin targets the energy loss is small compared with the beam energy, therefore the deviation Δt_i from the time-of-flight t_0 of the center of mass is also small. Writing $t_i=t_0+\Delta t_i$ in the equation above, we obtain after expanding to first order in powers of $\Delta t_i/t_0$,

$$\begin{aligned}\Delta E=E_0-E&=\frac{L^2}{2}\sum_{i}^{N} m_i\left[\left(\frac{1}{t_0}\right)^2-\left(\frac{1}{t_i}\right)^2\right]\\&=\frac{L^2}{2}\sum_{i}^{N} m_i\left[\left(\frac{1}{t_0}\right)^2-\left(\frac{1}{t_0+\Delta t_i}\right)^2\right]\\&=\left(\frac{L}{t_0}\right)^2\sum_{i}^{N} m_i\left\{\left(\frac{\Delta t_i}{t_0}\right)+O\left[\left(\frac{\Delta t_i}{t_0}\right)^2\right]\right\}\\&\simeq 2E_0\frac{1}{M}\sum_{i}^{N} m_i\left(\frac{\Delta t_i}{t_0}\right).\end{aligned}$$

M is the total mass of the cluster. The approximation above is justified since in the present experiment $\Delta t_i/t_0 \leqslant 1/100$. From above we get

$$\frac{\Delta E}{E_0}=2\frac{\Delta t}{t_0}, \tag{2}$$

where

$$\Delta t=\frac{1}{M}\sum_{I}^{N} m_i\Delta t_i=\frac{1}{N}\sum_{I}^{N}\Delta t_i. \tag{3}$$

The last equality was written for a homonuclear cluster. This gives an expression for the energy loss of the cluster in terms of the measured shift in time-of-flight Δt. The time-of-flight t_0 along the field-free region is calculated from

$$t_0=\sqrt{M/2E_0}L. \tag{4}$$

Consider now two thin targets of thicknesses Δx_i and Δx_j. The energy losses of the cluster in the targets are ΔE_i and ΔE_j, respectively. The deviations in time of the time of flight from that of the center of mass are Δt_i and Δt_j. Define the quantities $\delta x_{ij}=\Delta x_i-\Delta x_j$, $\delta E_{ij}=\Delta E_i-\Delta E_j$, and $\delta t_{ij}=\Delta t_i-\Delta t_j$. The energy loss δE_{ij} of the cluster after passing a target of thickness δx_{ij} is related to the difference in time-of-flight δt_{ij} in the same fashion as in Eq. (2),

$$\frac{\delta E_{ij}}{E}=2\frac{\delta t_{ij}}{t}. \tag{5}$$

E is the energy of the cluster at the entry of the jth target and it is related to the time-of-flight t in the same manner as in Eq. (4). The energy E (and consequently the time-of-flight t) is calculated by subtracting from E_0 the accumulated energy losses of the cluster after passing through all the targets preceding the jth target. The stopping power of the cluster is then calculated by

$$\left(\frac{dE}{dx}\right)_{ij}=\frac{\delta E_{ij}}{\delta x_{ij}}=2E\frac{\delta t_{ij}}{t\,\delta x_{ij}}. \tag{6}$$

It should be pointed out that the systematic error due to the uncertainty in the energy of the accelerator has been neglected in the above treatment, but has been taken into account in the stopping power ratio calculations. The values obtained in the present experiment are the energy loss of the cluster in a medium of thickness $\delta x_{ij}=\Delta x_i-\Delta x_j$ after passing a target of thickness Δx_j. This represents a ''differential'' measurement of the stopping power, which is different from the usual ''integral'' measurement done with energy sensitive detector techniques. Physically, our measurement probes the behavior of the energy deposition at a certain depth in the target, and not from the beginning of the target. However, the comparison with existing ''integral'' experiments or theories is straightforward. The overall time resolution of the above system is approximately 700 ps full width at half maximum (FWHM) (mainly due to MCP2).

An example of such a measurement is shown in Fig. 3 for 11.6-MeV B_3 passing through carbon foils of thicknesses $4.1\pm 0.2\ \mu g/cm^2$ and $12.9\pm 0.6\ \mu g/cm^2$. The time shift (1675 ± 85 ps) represents in this case an energy loss of $\delta E=150.7\pm 7.5$ keV.

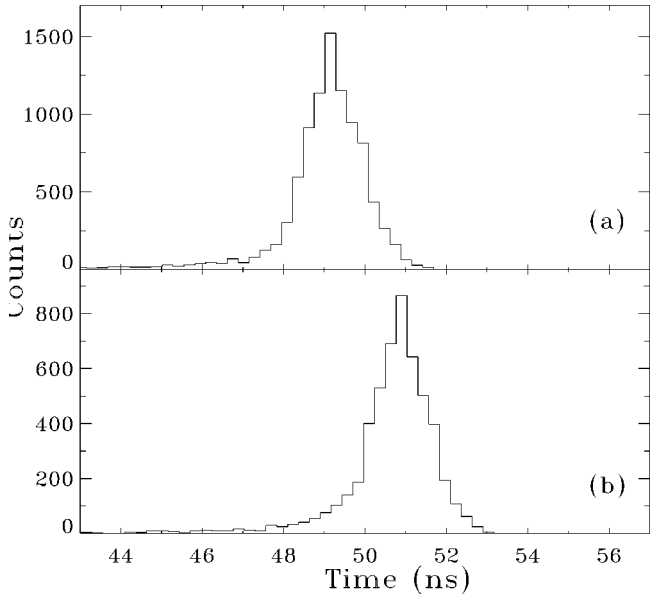

FIG. 3. Time-of-flight spectra (after delay) for 11.6-MeV B_3 passing through thin carbon foils of thicknesses of 4.1 ± 0.2 μg/cm^2 (a) and 12.9 ± 0.6 μg/cm^2 (b). The time shift (1675 ± 85 ps) represents in this case an energy loss of $\delta E=150.7\pm7.5$ keV.

C. Target thickness measurement

In order to extract precise values for the stopping power from time-of-flight measurements, it is very important to determine accurately the thickness of the foil used in the stopping power calculations [Eq. (6)]. Two different methods, which are described below, have been used. These two methods yield consistent results for target thicknesses thinner than 10 μg/cm^2, which are the target thicknesses of interest in this work.

1. Measurement of target thickness using multiple scattering

When a fast particle passes through a target, its direction of motion is influenced by collisions with target nuclei. This process is called multiple scattering and has been studied extensively for atomic particles passing through relatively thin targets (see [18] and references therein). The width of the angular distribution of the ions emerging from the target increases with increasing target thickness. For molecular projectiles, the angular distribution of the center of mass of the fragments has also been carefully characterized, using Monte Carlo simulation [18]. Although the multiple scattering distribution of a molecular projectile is a complex function of the target thickness, due to the correlation between the Coulomb explosion process inside the target and the multiple scattering, it has the advantage that in the present case, the values of target thicknesses can be obtained while performing the time-of-flight measurement.

Thus, in the present experiment, the target thicknesses were determined by measuring the width of the center-of-mass angular distribution of the molecular fragment ions using the position sensitive detector described in Sec. II B. The width of the distribution is then compared to a simulated width using an existing Monte Carlo simulation [18] in which the target thickness is used as a fitting parameter. Another advantage of this method is that it yields absolute target thickness, in contrast to the time-of-flight method described in the next section, which yields only a difference in target thicknesses, between two different targets. The values of the target thickness measured using the multiple scattering method were found to be independent of the molecular projectile identity (O_2, B_2, or C_3).

2. Measurement of target thickness using atomic energy loss

In this case, target thicknesses were deduced from energy-loss measurements of an atomic beam, using the time-of-flight setup described in Sec. II B. A beam of 11.6-MeV ^{28}Si was chosen for these measurements as its stopping power is well known [19] and is large enough to yield accurate values of target thicknesses. As a typical value, the energy change of the beam is about 20 keV per μg/cm^2 in a carbon target, yielding a time difference of 210 ps. As pointed out above, this method yields only the difference in target thickness between two targets, rather than their absolute values. This is due to the inability to measure absolute time of flight with the present setup.

Comparing the difference in target thicknesses between the methods described above yields consistent results for targets thinner than 10 μg/cm^2. However, discrepancies between the two techniques were found for thicker targets. This is due to the fact that the Monte Carlo code used for the simulation for the multiple scattering does not take into account the energy loss in the target, which changes the cross section for angular scattering. The values used in the present work are those obtained by the energy-loss measurement of Si. In order to obtain absolute values of target thicknesses, the thickness of the thinnest target obtained from the multiple scattering measurement has been used as a reference point.

III. EXPERIMENTAL RESULTS: STOPPING-POWER RATIOS

Energy-loss measurements were carried out for 11.3-MeV O_2 and 11.6-MeV B_3, C_3, and C_4, in carbon targets ranging in thickness from 4 to 50 μg/cm^2. The stopping-power ratio R, for a cluster X_n with n identical atoms of type X, is calculated as

$$R=\frac{(dE/dx)_{X_n|E=E_0}}{n(dE/dx)_{X|E=E_0/n}}, \tag{7}$$

where the atomic stopping powers for boron, carbon, and oxygen used in these calculations were taken from nuclear data tables [19]. As pointed out in Sec. II B, in this experiment, the energy loss ΔE can only be measured in a ''differential'' method, i.e., the values obtained are the energy loss in a target thickness δx after traversing a target that is Δx thick. The value δx is the difference between two adjacent target thicknesses Δx_1 and Δx_2:

$$\delta x=\Delta x_1-\Delta x_2. \tag{8}$$

The results obtained in the present experiments are displayed in Fig. 4 (solid circle) as a function of the target thickness $\Delta_x=(\Delta x_1+\Delta x_2)/2$, for 11.3-MeV O_2 [Fig. 4(a)], 11.6-MeV B_3 [Fig. 4(b)], 11.6-MeV C_3 [Fig. 4(c)], and 11.6-MeV C_4 [Fig. 4(d)]. Although the data do not show pronounced de-

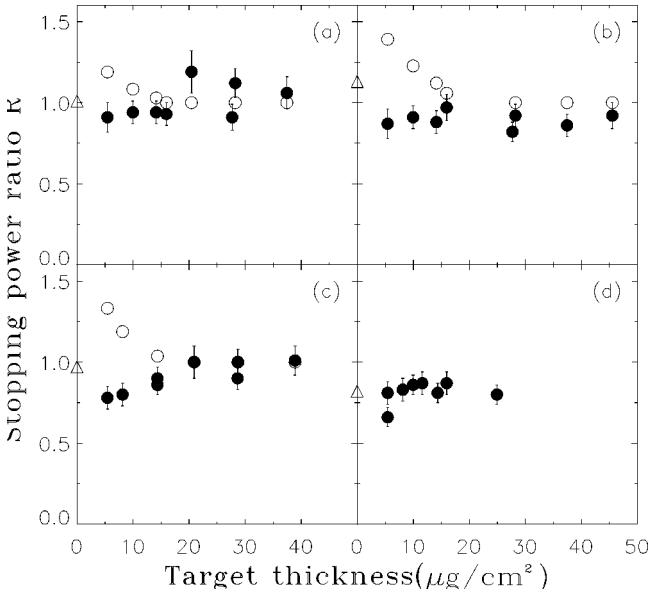

FIG. 4. Stopping-power ratios as a function of target thickness for 11.3 MeV O_2 (a), 11.6 MeV B_3 (b), 11.6-MeV C_3 (c), and 11.6-MeV C_4 (d): experimental (●), Arista model (○) and united-atom model (△).

viation from $R=1$, a slight deenhancement is clearly visible in the case of C_3 and C_4. The value of R tends towards unity as the target thickness increases for all projectiles, with the exception of C_4, where it is smaller than unity even for a thickness of 25 μg/cm^2.

IV. DISCUSSIONS

Enhancement effects in the stopping power of molecular projectiles are thought to be the results of the correlated motion of the atoms in the cluster, while passing through the solid. These effects can be readily explained when considering the Bethe formula for the electronic stopping power of a moving ion of charge Ze in matter [20],

$$\frac{dE}{dx}=\frac{4\pi Z^2e^4}{mv^2}ln\frac{2mv^2}{\hbar\langle\omega\rangle} \tag{9}$$

where m is the mass of the electron, v is the ion velocity, and $\hbar\langle\omega\rangle$ is the mean ionization potential of a target atom. If one assumes that a cluster of n charges Z_ie behaves as a point charge, the stopping-power ratio [see Eq. (7)] is given by

$$R=\frac{\left(\frac{dE}{dx}\right)_{\text{cluster}}}{\sum_{i=1}^{n}\left(\frac{dE}{dx}\right)_{\text{single ion}}}=\frac{\left(\sum_{i=1}^{n}Z_i\right)^2}{\sum_{i=1}^{n}Z_i^2}. \tag{10}$$

R is always greater than unity. Hence, enhancement effects are trivial results of the original stopping-power theory. Based on the above argument, the effect increases with increasing cluster size. However, it is obvious that the above description is rather crude, and a more detailed characterization of the correlation among the various fragments is needed.

In the following sections, two theoretical models will be used to describe the correlations between the cluster fragments. The first one, developed by Arista [3], takes into account the spatial correlation of the fragments, accounting for the vicinity effects on the energy loss of clusters in a free electron gas (Sec. IV A), while the second one, described in Sec. IV B is a very simple model, which we call the united-atom model, which in addition, takes into account the influence of the charge-state changes of the fragments on the cluster stopping power.

A. Energy loss of correlated particles

A theoretical model describing vicinity effects in the energy loss of a fast cluster of ions in a correlated motion has been developed, among others, by Arista [3], using a dielectric approach. In this formalism, the response of target electrons to the fields of the moving ions is described by a dielectric function $\epsilon(\mathbf{k},\omega)$ of the stopping medium, in the momentum-frequency space. The stopping power of a cluster of n charges Z_ie moving at velocity v is then given by

$$\frac{dE}{dx}=\sum_{i}^{n}Z_i^2S_p+\sum_{i\neq j}^{n}Z_iZ_jI(r_{ij}), \tag{11}$$

where r_{ij} is the internuclear separation of two ions in the cluster. Here S_p is the energy loss per unit length of a single proton having the same velocity as the cluster and is given by

$$S_p=\frac{2}{\pi v^2}\int_0^\infty\frac{dk}{k}\int_0^{kv}dwwIm\left[\frac{-1}{\epsilon(k,w)}\right]. \tag{12}$$

The interference function $I(r)$ given by

$$I(r)=\frac{2}{\pi v^2}\int_0^\infty dk\frac{\sin kr}{k^2r}\int_0^{kv}dwwIm\left[\frac{-1}{\epsilon(\mathbf{k},\mathbf{w})}\right] \tag{13}$$

describes the spatial correlations among the ions in the cluster. It becomes equal to S_p as $r_{ij}\to 0$ (the united-ion case) and goes to zero as $r_{ij}\to\infty$. Arista has applied this model to a free degenerate electron gas using a dielectric function derived by Lindhard [4]. In the present work, stopping power calculations were carried out for 11.3-MeV O_2 and 11.6-MeV B_3 and C_3 in carbon targets, using Arista's approach. In these calculations the carbon target is described by a dielectric function of a free degenerate electron gas with four free electrons per carbon atom. The configurations of the ions in the cluster at each stage of penetration [needed in Eq. (11)], were obtained using the Monte Carlo simulation described in Sec. II C 1 and in Ref. [18]. As pointed out above, this simulation includes the motion of the fragments due to their mutual Coulomb repulsion, as well as the multiple scattering due to the collisions with the target nuclei at the same time. The classical equations of motion of the particles are integrated along a path defined by the angles of scattering and the mutual screened Coulomb repulsion.

The stopping power ratios predicted by this model are shown in Fig. 4 (open circles), as a function of target thickness, together with the experimental results. Clearly, there is a strong disagreement between the theoretical values and the experimental results. Whereas the model predicts an enhancement effect in the energy loss for the cluster, an opposite effect or no effect at all is observed experimentally,

within the experimental accuracy. The reason for this discrepancy will be discussed in the following section.

B. The united-atom model

In the united-atom model that is introduced here, the cluster is treated as a united atom in which the cluster constituents have been unified. In this model, the cluster behaves as an atomic projectile, so that the stopping power for a cluster of n particles of atomic number z_i is given by the corresponding stopping power of an atom of atomic number $Z=\Sigma_{i=1}^{n}$.

In the section that follows, the physical foundation of this assumption and its domain of validity will be outlined. It is well known that for a stationary positive test charge embedded in a solid, the electrons of the solid respond by ''heaping up'' on the charge in such a way as to neutralize it and to screen out its field at distances large compared with the Debye length. The Debye length is proportional to the average electron velocity in the solid. If the positively charged ion travels at a velocity that is large compared with target electron velocities, the induced polarization charge lags behind the projectile and the screening distance becomes primarily determined by the velocity of the target electrons relative to the projectile. The dynamic screening length d in this case is given by $d=v/\omega_p$, where v is the ion velocity and ω_p is the plasma frequency of target electrons. Taking a simple expression for the screened potential of a moving ion, $\Phi(r)=(Ze/r)\exp[-r/d]$, we see that the degree of ionization and consequently the stopping power of the moving ion are determined by the ionic charge distribution through the screening length d.

This concept can be generalized to cluster projectiles, with the additional condition that the internuclear distances in the cluster need also to be compared to the dynamic screening length of the electrons in the target: as long as the internuclear distances are smaller than the screening length, the cluster can be considered an atomic particle, and its internuclear configuration is of no importance for stopping-power consideration.

What are the advantages of such a model, beyond its extreme simplicity, and why would such a model give better results than the more sophisticated calculations taking into account the correct spatial correlation? In the united-atom model, the correlation is of course taken to its limit, and is certainly not correct. But another very important aspect of the energy-loss process, which is dominant in the present regime of velocity, is corrected.

One of the additional assumptions in the calculations of molecular effects in stopping power that has been made is that the charge-state evolution of the molecular fragment ions inside the target does not differ from the case of single ions moving at the same velocity. However, it is well known that the charge-state distribution obtained for molecular fragments is lower than those obtained for individual ions at equivalent velocities. Such effects have been observed experimentally, for example, for 4.2-MeV N_2^+ ions impact upon carbon targets [21]. Final charge-state distributions for molecular ion impact show a marked shift towards lower charge states than in the case of monoatomic ion impact. The equilibrium length is also different for the two cases. Whereas the mean charge state for atomic ion impact is already equilibrated in moderately thin targets ($2\ \mu g/cm^2$), those measured for molecular ion impact are strongly dependent on the target thickness, even for thick targets ($20\ \mu g/cm^2$).

Thus, in addition to spatial correlation effects, which usually [but not always, because of the interference term in Eq. (11)] give rise to enhanced energy loss for the cluster relative to the individual atoms, there are charge-state molecular effects of an opposite sign, i.e., decreasing the stopping power of the cluster, due to the low charge states of the fragment ions inside the target. This means that the interference function in Eq. (11) should contain the correlations on charge-state evolution inside the target in addition to the correlations on stopping. This was already pointed out by Denton *et al.* in stopping-power calculations for H_3^+ [22] in carbon targets. In this case, however, it was assumed that the atomic equilibrium charge state ($Z_i=1$ for the proton in the H_3^+ case cited in Ref. [22]) was reached immediately for each of the constituents of the molecule.

In the united-atom model, the charge state of the cluster is assumed to be equal to the charge state of the equivalent united atom. Hence, the value of the stopping power of the united atom includes, in the limit of very small internuclear distances, both the spatial correlation and the correct (total) charge state for the cluster.

In fact, the lower charge states obtained with molecular projectiles as compared to atomic ones can be explained by the united-atom model if one uses, for example, the cross sections for electron loss σ_l and electron capture σ_c, as derived by Bohr [23] for projectiles of atomic number Z_p:

$$\sigma_l=\pi a_0^2 Z_t^{2/3} Z_p^{-1}\frac{v_0}{v}, \tag{14}$$

$$\sigma_c=4\pi a_0^2 Z_t^{1/3} Z_p^5\left(\frac{v_0}{v}\right)^6, \tag{15}$$

Here Z_t is the target atomic number, and a_0 and v_0 are the Bohr radius and velocity, respectively.

Comparing the cross sections for two projectiles of atomic numbers Z_{p1} and Z_{p2}, one obtains

$$\frac{\sigma_c(Z_{p1})}{\sigma_c(Z_{p2})}=\left(\frac{Z_{p1}}{Z_{p2}}\right)^5 \tag{16}$$

and

$$\frac{\sigma_l(Z_{p1})}{\sigma_l(Z_{p2})}=\frac{Z_{p2}}{Z_{p1}}, \tag{17}$$

demonstrating that the electron capture cross section grows much faster than the electron-loss cross section with increasing Z. Thus, in the united-atom model, for a cluster of n atoms, the total charge-state distribution will be lower due to the enhanced electron-capture cross section. The total effective charge of the cluster can be then deduced from the effective charge of the united atom. This united-atom model has in fact been applied successfully in many collision phenomena involving molecular ion projectiles as far as charge exchange processes are concerned [24–26].

In the framework of this model, the stopping-power ratio for a homonuclear cluster of N atoms is given by

$$R=\frac{(dE/dx)_{\text{cluster}}}{N(dE/dx)_{\text{single ion}}}=\frac{(dE/dx)_{\text{united atom}}}{N(dE/dx)_{\text{single ion}}}. \quad (18)$$

As an example, the stopping ratio of O_2 is calculated using the stopping power of sulfur:

$$R=\frac{(dE/dx)_{O_2}}{2(dE/dx)_{O}}=\frac{(dE/dx)_{S}}{2(dE/dx)_{O}}. \quad (19)$$

The necessary (atomic) value of the stopping power can be taken from energy-loss tables, or from theoretical calculations. Thus, this simple model automatically takes into account all the relevant processes for the stopping of clusters in solid matter, the charge-state evolution (as demonstrated above), as well as the spatial correlations among the cluster constituents. On the other hand, the values obtained using this model are, by definition, valid at the limit of very small target thicknesses, i.e., before the cluster dissociates into fragments with internuclear distances that are larger than the screening length d.

Stopping-power calculations have been carried out by using the united-atom model for the clusters that were measured in the present experiment (see Sec. III) i.e., for 11.3-MeV O_2, 11.6-MeV B_3, 11.6-MeV C_3, and C_4 at 11.6 MeV. The results are presented in Fig. 4 and are indicated by open triangles at the limit of zero target thickness. The values obtained are now close to $R=1$, which is in general agreement with the experimental data. Considering the simplicity of the model, the agreement is very satisfactory. The united-atom model can also be compared to previous experimental results. For example, Fig. 5 shows the results for the stopping-power ratio as a function of the dwell time in gold and carbon targets for H_2^+ and H_3^+ molecules as measured by Brandt, Ratkowski, and Ritchie [8]. Using the stopping power of He^+ and Li^+ ions [19] to stand for H_2^+ and H_3^+, respectively, one can calculate, using Eq. (18), the values of the stopping-power ratios. The results shown in Fig. 5 (open triangles) are in fair agreement with the existing experimental results, for very thin targets.

Another example is shown in Fig. 6 for the stopping power ratio of N_2^+ in carbon at energies between 0.5 to 1.8 MeV/atom in carbon targets as measured by Steuer *et al.* [12]. In this case, Si^+ was taken as the united-ion equivalent to an N_2^+ molecule for stopping-power calculations. Here again, a satisfactory agreement is obtained at the limit of zero thickness. It is interesting to note that in this case a deenhancement is obtained as in the experimental data, and that the value of the stopping-power ratio increases with increasing projectile energy in qualitative agreement with the experimental trend. Comparisons with additional previous data sets in the literature yield, in general, good agreement with the measured values [7,12].

Thus, in the united-atom model described above both enhancement and deenhancement effects can be obtained, and in general, it is the projectile velocity relative to the orbital velocities of its binding electrons that determines the stopping-power ratio. At low velocities (but still high enough that the screening length is larger than the internuclear distances), the low molecular charge states is the dominant factor, and reduction of the stopping power is expected. On the other hand, at high velocities, the cluster is highly ionized and enhancement will be observed. It is thus possible to use this model to predict the trend of the stopping-power ratios for fast clusters. Figure 7 shows, for example, the predicted trend for the stopping power ratio of C_2 in carbon target, as a function of the incident energy. For projectile energies below 300 keV/nucleon, a deenhancement is predicted, while an

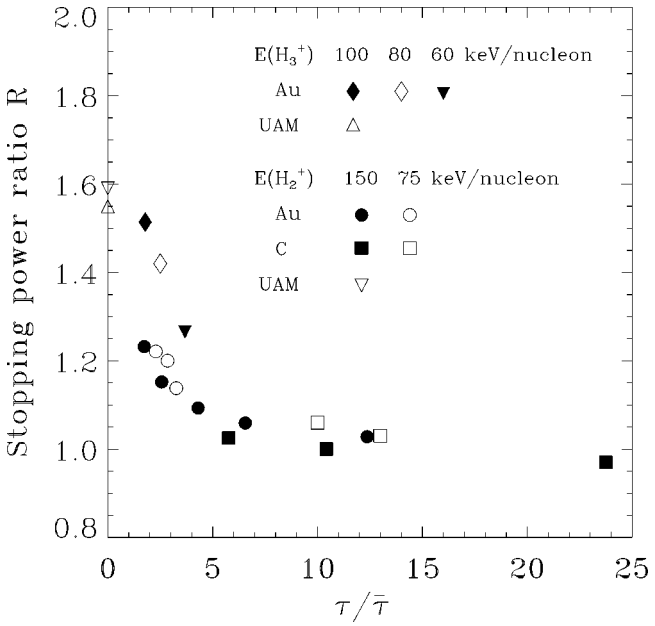

FIG. 5. Experimental data from Ref. [8] for the stopping-power ratios of H_2^+ and H_3^+ in carbon and gold targets, as a function of dwell time in the foil in units of $\bar{\tau}$. $\bar{\tau}$ is the average time required for the internuclear distance to become equal to $r_{\text{dist}}=v/\omega_p$ (see Ref. [8]). The results are compared to united-atom model (UAM) calculations for a gold target (open triangles).

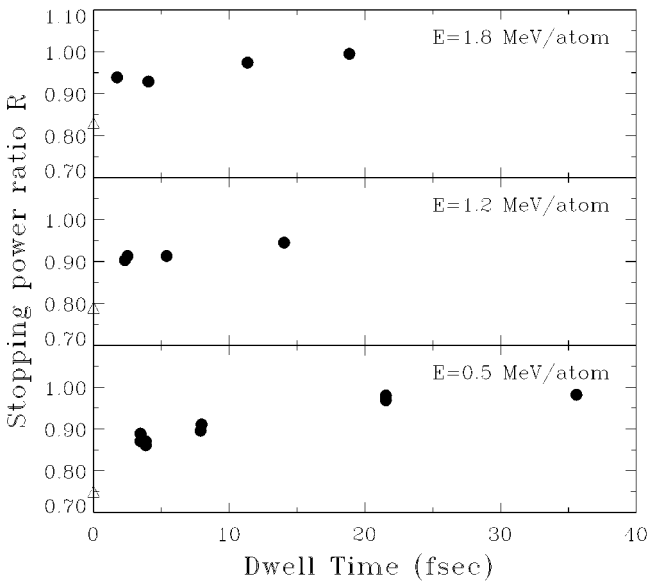

FIG. 6. Stopping-power ratios as a function of the dwell time in carbon targets for N_2^+ ions at energies of 0.5, 1.2, and 1.8 MeV/atom: experimental values from Ref. [10] (●) and united-atom model calculations (△).

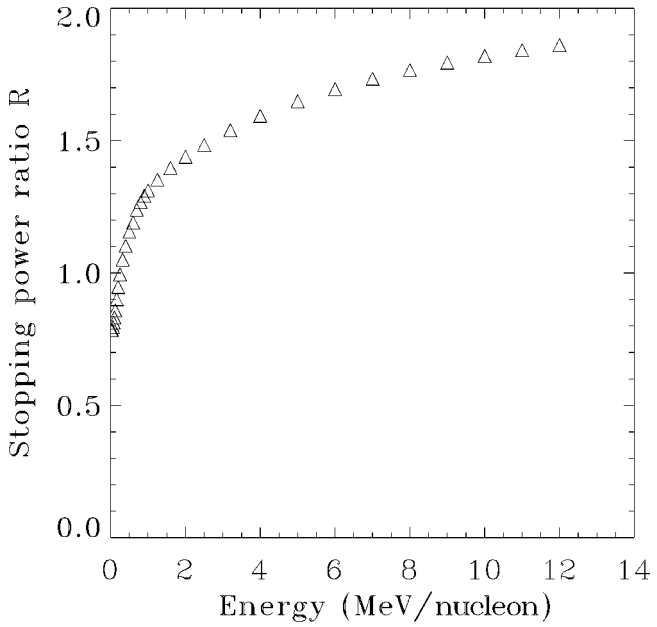

FIG. 7. Stopping-power ratio calculations using the united-atom model for C_2 as a function of energy.

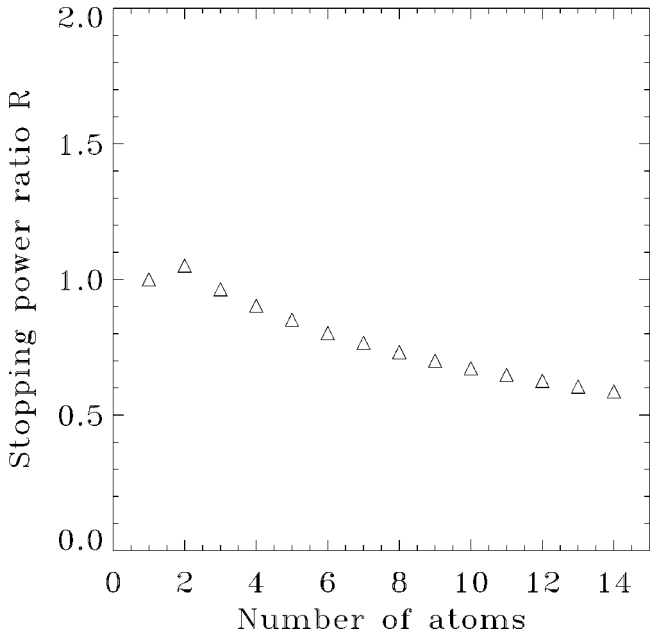

FIG. 8. Stopping-power ratio calculations using the united-atom model for carbon cluster C_n at energy of 320 keV/nucleon, as a function of the number of atoms in the cluster.

enhancement factor approaching the expected value of $R=2$ is achieved at high energies, i.e., when the molecule is highly ionized. Figure 8 shows the stopping power ratio as a function of the number of atoms in the cluster, for carbon clusters impinging at 320 keV/nucleon on a carbon target. As the number of atoms increases, the total charge state of the cluster decreases (at a constant velocity) and a stronger deenhancement is observed.

V. CONCLUSIONS

The stopping-power ratios of several simple clusters, in the velocity range of 3 to 4 Bohr velocity, have been measured using a time-of-flight method. The method is direct, and does not require corrections due to detector effects as in the case of standard energy-sensitive detection technique. Stopping-power ratios (R) close to unity were observed for O_2 and B_3 clusters, while the deenhancement effect is observed in the stopping power of C_3 and C_4 when compared to the sum of the stopping powers of the constituent atoms moving at the same velocity. A simple model describing the molecule in the early stages of penetration into the solid target, as a united atom, has been described. This model takes into account both the spatial correlation between the cluster constituents, and the enhanced capture cross section, which lowers the effective charge of the cluster inside the solid. It has been shown that this model explains the general trend of our experimental data as well as previous measurements of molecular stopping-power ratios. Preliminary calculations based on the united-atom model show that enhancement effect can be obtained only at very large velocities, when the cluster is rapidly stripped and the effective charge is high, a conclusion that has straightforward implications for the use of heavy-atom clusters for driving the initial step in the production of thermonuclear energy by the inertial confinement fusion process.

Note added in proof. A similar model as the one presented here was brought to our attention recently. The model [27] describes also the importance of the charge-state fluctuation on the energy loss of clusters. We thank Professor P. Signumd for his remarks.

ACKNOWLEDGMENTS

We would like to thank E. Nardi, Z. Zinamon, and M. Hass for fruitful discussions.

[1] C. Deutsch and N. A. Tahir, Nuovo Cimento A **106**, 1811 (1993).
[2] G. Basbas and R. H. Ritchie, Phys. Rev. A **25**, 1943 (1982).
[3] N. R. Arista, Phys. Rev. B **18**, 1 (1978).
[4] J. Lindhard, K. Dan. Vidensk. Selsk. Mat. Fys. Medd. **28**, 8 (1954).
[5] A. Perez, M. Döbeli, and H. A. Synal, Nucl. Instrum. Methods Phys. Res. B **88**, 25 (1994).
[6] K. B. Baudin, A. Brunelle, P. Chaurand, S. Della-Negra, J. Depauw, P. Hakansson, and Y. Le Beyec, Nucl. Instrum. Methods Phys. Res. B **88**, 61 (1994).
[7] E. Ray, R. Kirsch, H. H. Mikkelsen, J. C. Poizat, and J. Remillieux, Nucl. Instrum. Methods Phys. Res. B **69**, 133 (1992).
[8] W. Brandt, A. Ratkowski, and R. H. Ritchie, Phys. Rev. Lett. **33**, 1325 (1974).
[9] R. Laubert, IEEE Trans. Nucl. Sci. **26**, 1020 (1979).
[10] A. R. Nyaiesh, W. Steckelmacher, and M. W. Lucas, J. Phys. C **11**, 2917 (1978).

[11] J. C. Eckardt, G. Lantschner, N. R. Arista, and R. A. Baragiola, J. Phys. C **11**, L851 (1978).
[12] M. F. Steuer, D. S. Gemmel, E. P. Kanter, E. A. Johnson, and B. J. Zabransky, Nucl. Instrum. Methods **194**, 277 (1982).
[13] J. W. Tape, W. M. Gibson, J. Remillieux, R. Laubert, and H. E. Wegner, Nucl. Instrum. Methods **132**, 75 (1976).
[14] K. Baudin *et al.*, Nucl. Instrum. Methods Phys. Res. B **94**, 341 (1994).
[15] B. D. Wilkins, M. J. Fluss, S. B. Kaufman, C. E. Gross, and E. P. Steinberg, Nucl. Instrum. Methods **92**, 381 (1971).
[16] D. Kella *et al.*, Nucl. Instrum. Methods Phys. Res. A **329**, 440 (1993).
[17] Z. Vager, R. Naaman, and E. P. Kanter, Science **244**, 426 (1989).
[18] D. Zajfman, G. Both, E. P. Kanter, and Z. Vager, Phys. Rev. A **41**, 2482 (1990).
[19] L. C. Northcliffe and R. F. Schilling, Nucl. Data Tables A **7**, 233 (1970).
[20] H. Bethe, Ann. Phys. (Leipzig) **5**, 325 (1930).
[21] D. Maor, P. J. Cooney, A. Faibis, E. P. Kanter, W. Koenig, and B. J. Zabransky, Phys. Rev. A **32**, 105 (1985).
[22] C. Denton, F. J. Perez-Perez, I. Abril, R. Garcia-Molina, and N. R. Arista, Europhys. Lett. **35**, 499 (1996).
[23] N. Bohr, K. Dan. Vidensk. Selsk. Mat. Fys. Medd. **18**, (1948).
[24] D. Zajfman, Phys. Rev. A **42**, 5374 (1990).
[25] N. Cue, N. V. de Castro-Faria, M. J. Gaillard, J.-C. Poizat, J. Remillieux, D. S. Gemmel, and I. Plesser, Phys. Rev. Lett. **45**, 613 (1980).
[26] R. McCarroll, R. D. Piacentini, and A. Salin, J. Phys. B **3**, 137 (1970).
[27] P. Sigmund, J. S. Bitensky, and J. Jensen, Nucl. Instrum. Methods Phys. Res. B **112**, 1 (1996).